Recoverable and Self-healing Electromagnetic Wave Absorbing Nanocomposites

Xingyi Dai[a], Yuzhang Du[a], Jiye Yang[a], Ding Wang[b], Junwei Gu[a], Yifan Li[b], Steven Wang[c], Ben B. Xu[b]*, and Jie Kong[a]*

[a]MOE Key Laboratory of Materials Physics and Chemistry in Extraordinary Conditions, Shaanxi Key Laboratory of Macromolecular Science and Technology, School of Science, Northwestern Polytechnical University, Xi'an, 710072, P. R. China

[b]Mechanical and Construction Engineering, Faculty of Engineering and Environment, Northumbria University, Newcastle upon Tyne, NE1 8ST, UK

[c]School of Chemical Engineering and Advanced Materials, Newcastle University, Newcastle Upon Tyne, Tyne and Wear NE1 7RU, UK

*Corresponding Authors, E-mail: kongjie@nwpu.edu.cn(J.K.), ben.xu@northumbria.ac.uk(B.X.)

Abstract

Recent advancements in electronics engineering require materials with the resiliency and sustainability to extend their life time. With this regard, we presented a sustainable multi-functional nanocomposites strategy by introducing dynamic imine bonds based polyazomethine (PAM) as molecular interconnects and Fe_3O_4-loaded multiwalled carbon nanotubes as electromagnetic (EM) wave absorbing units. Driven by the reversible dynamic imine bonds, ourmaterials show robust spontaneous self-healing with excellent healing efficiencies of 95 % for PAM and 90 % for nanocomposite, and an acceleratedrecovery under a moderate mechanical stimulus. By adding Fe_3O_4-loaded multiwalled carbon nanotubes, the hybrids show excellent EM wave absorbing properties with 50% increment on minimum reflection coefficient (-40.6 dB) than the reported value. We demonstrate a full degradability by decomposing a nanocomposite sheet of 100 mg in an acidic solution within 90 min at room temperature. The nanofillers and monomers after degradation can be re-used to synthesis nanocomposites. The testing results for recoverable nanocomposites show a good retention on mechanical property. This novel strategy may shed a light on the downstream applications in EM wave absorbing devices and smart structures with great potential to accelerate circular economy.

Keywords: Self-healing; Reprocessing; Recycling; Electromagnetic wave absorption; Dynamic covalent bonds.

Graphic Abstract

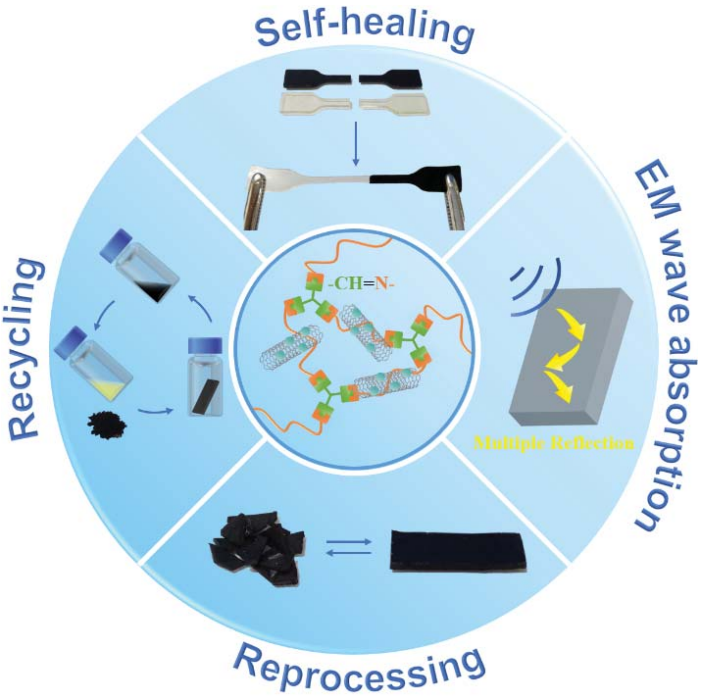

1. Introduction

Electromagnetic (EM) interference and pollution have been seen as threats to public health and environment, caused by the ubiquitously use of cell phones, motors, computers, remote sensors, radars, etc.[1,2] One of the essential solutions is to innovate and apply high performance EM wave absorbing materials in products, which has attracted considerable interests in last few years.[3-5] In comparison to other conventional materials (metals, ceramics and carbons), polymeric nanocomposites offer great advantages due to their flexibility, easy processing, light-weight, low cost, etc.[6-8] However, intrinsic characteristics from polymeric materials still bottle-necked the advancement where mechanical failures (cracking and fracture) can be easily found within structures/devices during operation.[9-12] The disposal of failed products arises even more concerns relevant to the environmental sustainability. Therefore, a circular material strategy that can provide resiliency, i.e. self-recovery and sustainability (recyclability), would be highly desirable for next generation EM wave absorbing devices.[13-15]

Self-healing property, fulfilled by the reversibility of macromolecular systems, has been studied extensively under noncovalent (physical) interactions, *i.e.* the inherent long-chain entanglements,[16] metal-ligand coordination,[17] host-guest interactions,[18,19] ionic interactions,[20] electrostatic interactions,[21] π-π stacking,[22] and hydrogen bonds.[23] Self-healing can be obtained by generating reversible chemical covalent bonds in the materials network,[24-27] those chemical interactions include acylhydrazone bonds,[28-30] disulfide bonds,[31,32] boronic ester linkages,[33] diarylbibenzofuranone links,[34] thiuram disulfide units,[35] Diels-Alder reactions,[36] and imine bonds (-CH=N-).[37-40]

Notably, Bao and co-workers synthesised a polydimethylsiloxane (PDMS) elastomer with spontaneous self-healing function by forming supramolecular dynamic interactions with coordination complexes.[41] Recently, Yu *et al.* developed a PDMS elastomer with self-healing property by incorporating imine bond, and demonstrated conceptual applications in flexible interconnector and chemical sensor.[42] Zhang *et al.* designed a kind of electromagnetic shielding materials with easy-processing and self-healing capacity under external force and magnetic force.[43] Wang *et al.* also reported an EM wave absorption coating with self-healing property, a less ideal minimum reflection coefficient was reported as -27.2 dB with a thickness of 4 mm.[44] Nevertheless, polymeric nanocomposites based EM absorbing materials with sustainable features has been under exploited, partially due to the high viscosity and irreversible physical interactions brought by the nanofillers.

In this work, we propose a synthesis strategy to achieve EM wave absorbing nanocomposites by using dynamic imine bonds-based polyazomethine (PAM) as macromolecular interconnects and Fe_3O_4-loaded multiwalled carbon nanotubes (Fe_3O_4@MWCNTs) as EM wave absorbing units. The nanocomposite presents a unique spontaneous self-healing, and an outstanding reprocessability that can be reformed under a low compressive stress at room temperature. We demonstrate a good sustainability for our composites by instantly degrading the polymer network in an acidic solution, from where the nanofillers and monomers can be collected and reused, therefore lead to an improved environmental impact by using this facile materials strategy.

2. Experimental Section

2.1. Materials

Trimethylolethane (98.0%, TCI), *p*-toluenesulfonylchioride (99.0%, TCI), 4-

dimethylaminopyridine (DMAP, 99.0%, Aladdin), 4-hydroxy benzaldehyde (99.0%, Aladdin), potassium carbonate (99.0%, Aladdin), poly(propylene glycol)bis(2-aminopropyl ether) (PEA, M_n=2000Da, Aladdin), iron(II) chloride tetrahydrate ($FeCl_2 \cdot 4H_2O$, 99.0%, Aladdin), iron chloride hexahydrate ($FeCl_3 \cdot 6H_2O$, 99.0%, Aladdin). Multi-walled carbon nanotubes (MWCNTs, average diameter of 20-40 nm, length of 10-30 um, purity > 90%) were purchased from Chengdu Org. Chem. Co. Ltd. All other reagents were utilized as received unless otherwise specified.

2.2. Two steps synthesis of 1, 1, 1-tris[(4-formylphenoxy)methyl]ethane

The first step is to synthesis tris[(4-tolylsulfonyl)methyl]ethane. As shown in in **Supporting Information** (**Fig. S1**), trimethylolethane (2.45g, 20 mmol) and a catalytic amount of DMAP were dissolved in 30 mL pyridine, then the mixture was cooled to 0 ^{o}C in an ice bath. Later, we added p-toluenesulfonylchioride (13.34g, 70 mmol) in 20 mL pyridine drop by drop into above mixture. The mixture was then removed from the ice-water bath and the reaction was kept going for 12 h at room temperature. When the reaction was completed, the mixture was diluted with 100 mL dichloromethane, and then washed with 200 mL 1 M HCl solution, 200 mL water and dried. The solvent was evaporated and a white crystalline solid was obtained by crystallization (9.8 g, yield: 84.1%). ^{1}H NMR (400 MHz, $CDCl_3$, δ): 7.72 (d, 6H, ArH), 7.38 (d, 6H, ArH), 3.79 (s, 6H, -CH2-), 2.49 (s, 9H, -CH3), 0.92 (s, 3H, -CH3).

The second step began with mixing tris[(4-tolylsulfonyl)methyl]ethane (5.83 g, 10 mmol), 4-hydroxy benzaldehyde (4.98 g, 40 mmol) and potassium carbonate (5.58 g, 40 mmol) in 30 mL anhydrous *N, N*-dimethylformamide (DMF) under nitrogen atmosphere, and the mixture was heated at 150 ^{o}C under reflux for 12 h. Then, the mixture was extracted into 100 mL dichloromethane and washed with 200 mL water, 100 mL saturated brine and dried over anhydrous $MgSO_4$. The solvent was evaporated and the crude product was achieved after purification (3.2 g, yield: 74.1%).

^{1}H NMR (400 MHz, $CDCl_3$, δ): 9.91 (s 3H, -CHO), 7.87 (d, 6H, ArH), 7.05 (d, 6H, ArH), 4.22 (s,6H, -CH2-), 1.41 (s, 3H, -CH3).

2.3. Preparations of polyazomethine (PAM) and Fe_3O_4@MWCNTs/*PAM nanocomposites*

For PAM sample preparation, poly(propylene glycol)bis(2-aminopropyl ether) (PEA, 200 mg, 0.1 mmol) was dissolved in 0.5 mL anhydrous *N, N*-dimethylformamide (DMF), followed by adding tris[(4-formylphenoxy)methyl]ethane (31 mg, 0.0667 mmol). After uniformly mixing the solution, glacial acetic acid (AcOH, 2.5 μL) was added. The mixture was then slowly transferred to the Teflon moulds and sealed at room temperature for 12 h. The prepared PAM was dried at 35 ^{o}C in the open air for 24 h, to allow the chemical cross-linking to complete within the materials. Fe_3O_4 decorated multi-walled carbon nanotubes (Fe_3O_4@MWCNTs) were prepared as presented in **Fig. S2**. For Fe_3O_4@MWCNTs/PAM nanocomposites, certain amount of synthesised Fe_3O_4@MWCNTs nanofillers were added and ultra-sonicated for 30 min when mixing PEA and tris[(4-formylphenoxy)methyl]ethane in DMF. The rest processes were the same to that for PAM.

2.4. Characterization

^{1}H NMR analyses were recorded by a Bruker Avance 400 spectrometer (Bruker BioSpin, Switzerland) at 25 ^{o}C with deuterated chloroform ($CDCl_3$) as the solvent. Chemical shifts are referenced to tetramethylsilane (TMS).The uniaxial tensile tests were carried out following the requirements in ISO37-4, using an Instron 3342 universal tester at a crosshead speed of 20 mm min^{-1}. At least four specimens for each healing time and repeated repair were tested to obtain the average values of the tensile strength, fracture strain, as well as standard deviation. Optical observations were performed under an upright microscope (Olympus IX73). The surface microstructures were assessed *via* a field emission scanning electron microscope (FE-

SEM, SU-8010, Hitachi) operated at an accelerating voltage of 1.0 kV. The surface profiles were performed with a Dektak XT (Bruker) with a line scanning rate of 0.05 mm per second.Other analyses, such as Fourier transform infrared spectroscopy, Powder X-ray diffraction, X-ray photoelectron spectroscopy are presented in **Supporting Information**.

2.5. Microwave absorption measurements and analysis

The relative complex permittivity and permeability were measured on rectangular specimens (22.8 mm × 10.2 mm × 2.0 mm) by a vector network analyzer (VNA, MS4644A, Anritsu, Japan) using waveguide method in the frequency range of 8.2–12.4 GHz. On the basis of the metal backplane model, the reflection coefficient (RC) can be calculated from the measured relative complex permittivity and permeability according to the transmission line theory by the following equations:

$$RC = 20\log_{10}\left|\frac{Z_{in}-1}{Z_{in}+1}\right| \qquad \text{(Equ. 1)}$$

$$Z_{in} = \sqrt{\frac{\mu_r}{\varepsilon_r}}\tanh\left[j\frac{2\pi fd}{c}\sqrt{\mu_r\varepsilon_r}\right] \qquad \text{(Equ. 2)}$$

where Z_{in} stands the normalized input impedance, μ_r and ε_r are, respectively, the relative complex permeability and permittivity, and f represents the frequency of the microwaves, d is the thickness of tested materials, and c is the light velocity in vacuum.[45,46]

3. Results and Discussion

The reversible dynamic imine bond enabled self-healing process is illustrated in **Fig. 1a**. The key molecular interconnect is the dynamic A_2-B_3 imine bonds based cross-linked PAM network, where A_2 and B_3 represent poly(propylene glycol)bis(2-aminopropyl ether) and 1, 1, 1-tris[(4-formylphenoxy)methyl]ethane, respectively. The formation of dynamic imine bond (-CH=N-) can be traced from the ^{1}H NMR results (**Fig. S3**) with a signature peak signalling at 8.24 ppm. This also agrees well

with the FT-IR data (**Fig. S4**), where a new absorption peak for -CH=N- bond was found at 1640 cm^{-1}.

To assess the self-healing performance enabled by the dynamicimine bonds, pure PAM tileswith shapes as '*Tetris*' elements (**Fig. 1b**) are prepared and assembled into a rectangular sheet at free-standing state, then left to heal in an open air at 25 °C. Interestingly, the '*Tetris*' tiles spontaneously splice together into one single sheet after 24 h, without applying any external stimuli. We subsequently perform a quick assessment for the spliced sheet under a uniaxial compression, the flat sheet transforms into a buckling state (**Fig. 1c**), and it also can be stretched (**Movie S1**), which indicates a good homogeneity for the healed sample. Optical microscopic observations were used to record the spontaneous self-healing on the surface of pure PAM. A nearly full restoration of surface can be observed (**Fig. 1d**) after a healing process for 24 h (**Fig. 1e**). The surface profiles in **Fig. 1f** describe the out of plane morphological changes for specimens (0.8 mm in thickness) during self-healing. The dash line represents the true cut profiles that can't be reflected due to the instrumental limit from the probe. After self-healing,the surfaceis reinstated with negligible residual depths of less than 2 μm.

We next study the self-healing property quantitatively by measuring the uniaxial tensile stress-strain relationship as a function of healing time at 25 °C (**Fig. 1g**). For the as-fabricated sample (or original sample), the results suggest a Young's modulus (E_{pure}) of ~ 0.76±0.08 MPa, a breaking strain of 215 % and peak strength of 0.79 MPa for pure PAM. The healing efficiency is defined as η_s/η_o, where η_s is the fracture strain for current sample, and η_o is the fracture strain for original sample. The healing efficiency results indicate a clear dependency on the healing time, the elongations reach ~ 100 % of that for the original PAM sample after healing for 24 h.

It was found that the specimens healed for 6 h and 12 h broke at the incision, while the specimen healed for 24 h did not break at the contacted surfaceunder the tensile testing. This observation further confirmed that the mechanical properties of PAM can be completely restored after a certain period of self-repair and PAM has excellent self-repairing characteristics. Cyclic tensile test was performed to verify the robustness of this self-healing effect, where sample was cut into two parts from the middle and performed the spontaneous self-healing for 24 h for each cycle. The stress-strain curves in **Fig. 1h** indicate robust self-healing performances for both of pure PAM by showing a η_s/η_o of 95 % for PAM after three cycles (H3). The reversible nature of dynamic imine bonds plays a key role in this remarkable self-healing function. The 'mobile' ends between scratched surfaces, -NH_2 groups and -CH=O groups, spontaneously couple to form -CH=N- bonds when the surfaces physically contact, therefore led to a self-healing functionality.[47-49]

To explore the EM absorbing application for this unique PAM materials, Fe_3O_4@MWCNTs/PAM nanocomposites was fabricated, as illustrated in (**Fig. 2a**). In addition, refining the compatibility between the fillers and polymer matrix is the key issue to improve the absorption performance of composites. By modifying the CNTs with Fe_3O_4, the aggregation of CNTs could be avoided due to the presence of Fe_3O_4 magnetic nanoparticles on its surface, which effectively decreased the Vander Waals' interactions between CNTs, meanwhile the intrinsic aggregation of Fe_3O_4 magnetic nanoparticles will be prevented since the existence of CNTs.Thus, Fe_3O_4@MWCNTs nanocomposites could uniformly disperse in the polymer matrix for the synergy between Fe_3O_4 and CNTs. By taking advantage of coupling the imine bonds on the surface, we even weld pure PAM and nanocomposite samples together (**Fig. 2b**) and demonstrate a good elasticity for the welded sample under stretching (**Fig. S7** and **Movie S2**) and bending. A brief test to verify the bonding strength after

the formation of dynamic imine bonds between surfaces of pure PAM and nanocomposite with 15 wt% Fe_3O_4@MWCNTs films (1 mm in thickness, 0.2 g in weight for each film, **Fig. 2c**), the alien films bond so tight that the bilayer can hold a shear load of 200 g, five hundred folds of the weight for bilayer film.

In tensile testing section, the data from 15 wt% Fe_3O_4@MWCNTs/PAM nanocomposite is selected. For the as-fabricated samples (or original samples), the results suggest a Young's modulus (E_{comp}) of ~ 2.25±0.22 MPa, a breaking strain of 192% and peak strength of 3.07 MPa for the nanocomposites with 15 wt% Fe_3O_4@MWCNTs. As noticed, the enhancement in Young's module, E_{comp}/E_{pure} ~ 3, shows a considerable gap to the calculated value (E_{comp}/E_{pure}~ 62) based on Halpin and Tsai's equations,[50,51] because of the decreasing of physical interaction area after coating Fe_3O_4 particles on the surface of MWCNT.Similar to Pure PAM sample, a high healing efficiency, η_s/η_o~ 98 %, was shown (**Fig. 2d**) for nanocomposites sample with 15 wt% Fe_3O_4@MWCNTs after healing for 24 h. Further cyclic test results indicate robust self-healing performances for the same nanocomposite with a η_s/η_o of 90 % after three cycles (H3).

The EM wave absorbing property of materials, mainly determined by the Fe_3O_4@MWCNTs nanoparticles in matrix, are generally associated with their electromagnetic parameters, *i.e.* relative complex permittivity (□$_r$ = □□ - j□□) and relative complex permeability (μ_r = μ□ - $j\mu$□), where the real parts (ε' and μ') represent the storage ability of EM wave and imaginary parts (ε'' and μ'') are related to dissipation of EM wave.[52] Recent theoretical development on the EM wave absorptionalso proposed a hypothesis that an enhancement of absorption (**Fig. 2f**) can be achieved by creating a multiple reflection state within the materials when uniformly distributing nanoparticles inmatrix.[53,54]

When measuring the complex permittivity and permeability for the nanocomposites (**Fig. S5**), we found that both □□ and □□ values significantly increased in X-band (8.2–12.4 GHz) as the concentration of Fe_3O_4@MWCNTs increases. A high value of μ'', strong dielectric loss and magnetic loss properties were achieved for the composite with 15 wt% nanofillers (**Fig. S5c** and **S5f**). By calculating the reflection coefficient (RC) *via* the transmission line theory (**Equ.1 & 2**), the nanocomposite with 15 wt% Fe_3O_4@MWCNT shold the strongest EM wave absorptions with a minimum RC to -40.6 dB at 10.0 GHz (**Fig. 2g-i**), 150% of the value in the previous report.[44] The effective absorption bandwidth is much higher (3.4 GHz) to cover 81% X-band. This significant enhancement could be attributed to the minimal reflection on the PAM surface (low $\varepsilon' \sim 3$) benefited from good impedance matching. And the Fe_3O_4@MWCNTs attenuates the EM waves with the complementary effect between dielectric loss and magnetic loss over a wide range of frequency. The strong dielectric loss is attributed to electron polarization relaxation and interfacial polarizations between Fe_3O_4 and MWCNTs, and between MWCNTs and PAM matrix. The Fe_3O_4 nanoparticles make a contribution to the magnetic loss, which is mainly induced by the natural resonance and eddy current loss. It should be noted thatthe uniformly distribution of Fe_3O_4@MWCNTs can lead to multiple reflections of EM wave, thus further strengthen EM wave absorption performancefor the nanocomposite.[55,56]

The dynamic imine bonds also offer a unique reprocessability to our materials with a moderate mechanical compression. To demonstrate this feature, coloured pure PAM pieces (dimensional size less than 1 cm×1 cm, 1 mm in thickness, see inset in **Fig. 3a**) are cut and put into a mould. After being compressed under 5 MPa for 3 h at 25 °C, all pieces re-united into one single sheet. To further understand this mechano-reformation process, we performed time dependent reformation experiments with different compression stresses (up to 10 MPa). Surprisingly, it only took 1 h to

achieve a full reformation when applying 10 MPa. The reformation for 15% Fe_3O_4@MWCNTs nanocomposites took slightly longer (**Fig. 3b**) than Pure PAM at the same compression stress. The tensile results for reformed samples (**Fig. 3c** and **3d**) suggest a good retention of mechanical property for both pure PAM and nanocomposites with 15 wt% Fe_3O_4@MWCNTs, after the fourth reprocessing cycle (R4).

In addition to the good self-healing and mechano-reformation capabilities, the dynamicbond also enables an outstanding recyclability, where the organic network of composite can be fully decomposed by decoupling the -CH=N- bondsin an acidic solution (**Fig.3e**), such as glacial acetic acid, hydrochloric acid and trifluoroacetic acid. At a solution of HCl/DMF (2 v/v %), purePAM film (~ 100 mg, **Fig.S6**) can be instantly degraded within 2.5 h, rather than swelling in pure DMF. The ^{1}H NMR data for the post-degradation solution for PAM (**Fig. 3f**), reveals a complete degradation of PAM network, the imine proton peak for -CH=N- at 8.24 ppm disappears and the characteristic signal of end aldehyde groups at 9.86 ppm becomes stronger than that of PAM.

We further study the degradation efficiency by measuring the weight loss as a function of the acid concentration. The t_{total} (time for degrading all polymeric phase in sample, **Fig. 3g**) for nanocomposite with 15 wt% Fe_3O_4@MWCNTs takes about 80 % of the t_{total} for pure PAM at the same acid concentration. The kinetics data indicates that the $t_{1/2}$ (time for degrading 50 wt% polymer in sample) takes ~ 70 % of t_{total} for pure PAM and ~ 80 % of t_{total} for nanocomposite with 15 wt% Fe_3O_4@MWCNTs, due to the decreased physical contact area as a result of the volumetric blocking by the nanofillers. When increasing the acid concentration to 5 v/v%, the degradation reaches an instant level by showing a $t_{1/2}$ less than 50 min for pure PAM and a $t_{1/2}$ less

than 60 min for nanocomposite with 15 wt% Fe_3O_4@MWCNTs. After full decomposition, we re-synthesised the nanocomposite from the recycled components. After assessing the mechanical property, we found that the recycled nanocomposite (**Fig. 3h**) maintains a similar fracture strain, maximum stress and shows a slightly low young's modules ($E_{recycled}/E_o$ ~ 80 %), comparing to the original samples.

3. Conclusion

In summary, we propose a dynamic imine bond enable resilient and circular materials strategy with potentials in EM wave absorbing application. The synthesised materials show unique self-healing feature and robust reprocessing capability driven by the dynamic imine bonds based molecular interconnects. By adding Fe_3O_4@MWCNTs, excellent EM wave absorbing property was achieved with 50% of enhancement on the EM wave absorption. Moreover, a highly efficient recyclability is demonstrated by instantly dissolving PAM based materials in an acidic solution within 1.5 h, by de-coupling the molecular interconnects. After separation, the nanofillers and monomers can be reused, therefore lead to a good environmental sustainability. We expect this molecular interconnect enabled sustainable nanocomposites technology to find applications in the fields of flexible electronics, micro-devices and smart structures.

Associated Content

Supporting Information

^{1}H NMR and FT-IR spectra of polymers; permittivity, permeability, dielectric tangent lossvalues, and magnetic tangent loss values of Fe_3O_4@MWCNTs/PAM nanocomposites; swelling ratio and mass loss of PAM; XRD and XPS spectra of MWCNTs, Fe_3O_4@MWCNTs.

Acknowledgements

This work was financially supported by the National Natural Science Foundation of China through grants (21875190, 21374089), Shaanxi Natural Science Funds for Distinguished Young Scholars (2018JC-008) and the Engineering and Physical Sciences Research Council (EPSRC) grant from UK -EP/N007921/1 and EP/N032861/1.

References:

[1] A. P. Singh, M. Mishra, P. Sambyal, B. K. Gupta, B. P. Singh, A. Chandra, S. K. Dhawan, Encapsulation of γ-Fe_2O_3 decorated reduced graphene oxide in polyaniline core-shell tubes as an exceptional tracker for electromagnetic environmental pollution, J. Mater. Chem. A 2 (2014) 3581-3593.

[2] S. Xiao, H. Mei, D. Han, K. G. Dassios, L. Cheng, Ultralight lamellar amorphous carbon foam nanostructured by SiC nanowires for tunable electromagnetic wave absorption, Carbon 122 (2017) 718-725.

[3] C. Luo, W. Duan, X. Yin, J. Kong, Microwave-absorbing polymer-derived ceramics from cobalt-coordinated poly(dimethylsilyiene)diacetylenes, J. Phys. Chem. C 120 (2016) 18721-18732.

[4] N. Yousefi, X. Sun, X. Lin, X. Shen, J. Jia, B. Zhang, B. Tang, M. Chan, J. Kim, Highly aligned graphene/polymer nanocomposites with excellent dielectric properties for high-performance electromagnetic interference shielding, Adv. Mater. 26 (2014) 5480-5487.

[5] F. Shahzad, M. Alhabeb, C. B. Hatter, B. Anasori, S. M. Hong, C. M. Koo, Y. Gogotsi, Electromagnetic interference shielding with 2D transition metal carbides (MXenes), Science 353 (2016) 1137-1140.

[6] Z. Chen, C. Xu, C. Ma, W. Ren, H. Cheng, Lightweight and flexible graphene foam composites for high-performance electromagnetic interference shielding, Adv. Mater. 25 (2013) 1296-1300.

[7] H. Lv, Y. Guo, Z. Yang, Y. Cheng, L. P. Wang, B. Zhang, Y. Zhao, Z. J. Xu, G. Ji, A brief introduction to the fabrication and synthesis of graphene based composites for the realization of electromagnetic absorbing materials, J. Mater. Chem. C 5 (2017) 491-512.

[8] I. Arief, S. Biswas, S. Bose, FeCo-anchored reduced graphene oxide framework-based soft composites containing carbon nanotubes as highly efficient microwave absorbers with excellent heat dissipation ability, ACS Appl. Mater. Interfaces 9 (2017) 19202-19214.

[9] T. Huynh, P. Sonar, H. Haick, Advanced materials for use in soft self-healing devices, Adv. Mater. 29 (2017)1604973.

[10] Z. Zou, C. Zhu, Y. Li, X. Lei, W. Zhang, J. Xiao, Rehealable, fully recyclable, and malleable electronic skin enabled by dynamic covalent thermoset nanocomposite, *Sci. Adv*. 4 (2018) eaaq0508.

[11] W. Yang, B. Shao, T. Liu, Y. Zhang, R. Huang, F. Chen, Q. Fu, Robust and mechanically and electrically self-healing hydrogel for efficient electromagnetic interference shielding, ACS Appl. Mater. Interfaces 10 (2018) 8245-8257.

[12] D. Y. Wu, S. Meure, D. Solomon, Self-healing polymeric materials: A review of recent developments, Prog. Polym. Sci. 33 (2008) 479-522.

[13] H. Lv, Z. Yang, P. L. Wang, G. Ji, J. Song, L. Zheng, H. Zeng, Z. Xu, A voltage-boosting strategy enabling a low-frequency, flexible electromagnetic wave absorption device, Adv. Mater. 30 (2018) 1706343.

[14] C. Luo, T. Jiao, Y. Tang, J. Kong, Excellent electromagnetic wave absorption of iron-containing SiBCN ceramics at 1158 K high-temperature, Adv. Eng. Mater. 20 (2018) 1701168.

[15] X. Gao, J. Li, Y. Gao, S. Guo, H. Wu, R. Chen, Microwave absorbing properties of alternating multilayer composites consisting of poly(vinyl chloride) and multi-walled carbon nanotube filled poly(vinyl chloride) layers, Compos. Sci. Technol. 130 (2016) 10-19.

[16] B. J. Blaiszik, S. L. B. Kramer, S. C. Olugebefola, J. S. Moore, N. R. Sottos, S. R. White, Self-Healing Polymers and Composites, Annu. Rev. Mater. Res. 40(2010)179-211.

[17] G. Weng, S. Thanneeru, J. He, Dynamic coordination of Eu-iminodiacetate to control fluorochromicresponse of polymer hydrogels to multistimuli, Adv. Mater. 30 (2018)1706526.

[18] M. Nakahata, Y. Takashima, H. Yamaguchi, A. Harada, Redox-responsive self-healing materials formed from host-guest polymers, Nat. Commun. 2 (2011)511.

[19] K. Miyamae, M. Nakahata, Y. Takashima, A. Harada, Self-healing, expansion-contraction, and shape-memory properties of a preorganized supramolecular hydrogel through host-guest interactions, Angew. Chem. Int. Ed. 54 (2015) 8984-8987.

[20] A. Das, A. Sallat, F. Boehme, M. Suckow, D. Basu, S. Wiessner, K. W. Stoeckelhuber, B. Voit, G. Heinrich, Ionic modification turns commercial rubber into a self-healing material, ACS Appl. Mater. Interfaces 7 (2015) 20623-20630.

[21] T. L. Sun, T. Kurokawa, S. Kuroda, A. Bin Ihsan, T. Akasaki, K. Sato, M. A. Haque, T. Nakajima, J. P. Gong, Physical hydrogels composed of polyampholytes demonstrate high toughness and viscoelasticity, Nat. Mater. 12 (2013) 932-937.

[22] J. Fox, J. J. Wie, B. W. Greenland, S. Burattini, W. Hayes, H. M. Colquhoun, M. E. Mackay, S. J. Rowan, High-strength, healable, supramolecular polymer nanocomposites, J. Am. Chem. Soc. 134 (2012) 5362-5368.

[23] Y. Chen, A. M. Kushner, G. A. Williams, Z. Guan, Multiphase design of autonomic self-healing thermoplastic elastomers, Nat. Chem. 4 (2012) 467-472.

[24] S. J. Rowan, S. J. Cantrill, G. Cousins, J. Sanders, J. F. Stoddart, Dynamic covalent chemistry, Angew. Chem. Int. Ed. 41 (2002) 898-952.

[25] R. J. Wojtecki, M. A. Meador, S. J. Rowan, Using the dynamic bond to access macroscopically responsive structurally dynamic polymers, Nat. Mater. 10 (2011) 14-27.

[26] Z. Wei, J. H. Yang, J. Zhou, F. Xu, M. Zrinyi, P. H. Dussault, Y. Osada, Y. M. Chen, Self-healing gels based on constitutional dynamic chemistry and their potential applications, Chem. Soc. Rev. 43 (2014) 8114-8131.

[27] N. Roy, B. Bruchmann, J.-M. Lehn, Dynamers: dynamic polymers as self-healing materials, Chem. Soc. Rev. 44 (2015) 3786-3807.

[28] G. Deng, C. Tang, F. Li, H. Jiang, Y. Chen, Covalent cross-linked polymer gels with reversible sol-gel transition and self-healing properties, Macromolecules 43 (2010) 1191-1194.

[29] X. Yang, G. Liu, L. Peng, J. Guo, L. Tao, J. Yuan, C. Chang, Y. Wei, L. Zhang, Highly efficient self-healable and dual responsive cellulose-based hydrogels for controlled release and 3D cell culture, Adv. Funct. Mater. 27 (2017)1703174.

[30] P. Wang, G. Deng, L. Zhou, Z. Li, Y. Chen, Ultrastretchable, self-healable hydrogels based on dynamic covalent bonding and triblock copolymer micellization, ACS Macro Lett. 6 (2017) 881-886.

[31] A. Rekondo, R. Martin, A. Ruiz De Luzuriaga, G. Cabanero, H. J. Grande, I. Odriozola, Catalyst-free room-temperature self-healing elastomers based on aromatic disulfide metathesis, Mater. Horiz. 1 (2014) 237-240.

[32] S.-M. Kim, S.-H. Jeon, S.-A. Shin, S. Park, J. Jegal, S. Y. Hwang, D. X. Oh, J. Park, Superior toughness and fast self-healing at room temperature engineered by transparent elastomers, Adv. Mater. 30 (2018)1705145.

[33] O. R. Cromwell, J. Chung, Z. Guan, Malleable and self-healing covalent polymer networks through tunable dynamic boronic ester bonds, J. Am. Chem. Soc. 137 (2015) 6492-6495.

[34] K. Imato, M. Nishihara, T. Kanehara, Y. Amamoto, A. Takahara, H. Otsuka, Self-healing of chemical gels cross-linked by diarylbibenzofuranone-based trigger-free dynamic covalent bonds at room temperature, Angew. Chem. Int. Ed. 51 (2012) 1138-1142.

[35] Y. Amamoto, H. Otsuka, A. Takahara, K. Matyjaszewski, Self-healing of covalently cross-linked polymers by reshuffling thiuram disulfide moieties in air under visible light, Adv. Mater. 24 (2012) 3975-3980.

[36] K. K. Oehlenschlaeger, J. O. Mueller, J. Brandt, S. Hilf, A. Lederer, M. Wilhelm, R. Graf, M. L. Coote, F. G. Schmidt, C. Barner-Kowollik, Adaptable hetero Diels-Alder networks for fast self-healing under mild conditions, Adv. Mater. 26 (2014) 3561-3566.

[37] M. E. Belowich, J. F. Stoddart, Dynamic imine chemistry, Chem. Soc. Rev. 41 (2012) 2003-2024.

[38] B. Yan, J. Huang, L. Han, L. Gong, L. Li, J. N. Israelachvili, H. Zeng, Duplicating dynamic strain-stiffening behavior and nanomechanics of biological tissues in a synthetic self-healing flexible network hydrogel, ACS Nano 11 (2017) 11074-11081.

[39] J. Ahner, M. Micheel, R. Geitner, M. Schmitt, J. Popp, B. Dietzek, M. D. Hager, Self-healing functional polymers: optical property recovery of conjugated polymer films by uncatalyzed imine metathesis, Macromolecules 50 (2017) 3790-3796.

[40] Y. Liu, Z. Tang, Y. Chen, S. Wu, B. Guo, Programming dynamic imine bond into elastomer/graphene composite toward mechanically strong, malleable, and multi-stimuli responsive vitrimer, Compos. Sci. Technol. 168 (2018), 214-223.

[41] X. Yan, Z. Liu, Q. Zhang, J. Lopez, H. Wang, H. Wu, S. Niu, H. Yan, S. Wang, T. Lei, J. Li, D. Qi, P. Huang, J. Huang, Y. Zhang, Y. Wang, G. Li, J. B. H. Tok, X. Chen, Z. Bao, Quadruple H-bonding cross-linked supramolecular polymeric materials as substrates for stretchable, antitearing, and self-healable thin film electrodes, J. Am. Chem. Soc. 140 (2018) 5280-5289.

[42] B. Zhang, P. Zhang, H. Zhang, C. Yan, Z. Zheng, B. Wu, Y. Yu, A transparent, highly stretchable, autonomous self-healing poly(dimethyl siloxane) elastomer, Macromol. Rapid Commun. 38 (2017)1700110.

[43] H. Zhang, H. Han, X. Xu, Dynamic and regional constructive electromagnetic protecting materials made by MWNT/Fe_3O_4/poly pyrrole doped vitrimers, Compos. Sci. Technol. 158 (2018), 61-66.

[44] Y. Wang, M. Pan, X. Liang, B. Li, S. Zhang, Electromagnetic wave absorption coating material with self-healing properties, Macromol. Rapid Commun. 38 (2017)1700447.

[45] C. Luo, T. Jiao, J. Gu, Y. Tang, J. Kong, Graphene Shieled by SiBCN Ceramic: A Promising High Temperature Electromagnetic Wave-Absorbing Material with Oxidation Resistance, ACS Appl. Mater. Interfaces, 10 (2018) 39307-39318

[46] C. Luo, Y. Tang, T. Jiao, J. Kong, High-temperature stable and metal-free electromagnetic wave-absorbing SiBCN ceramics derived from carbon-rich

hyperbranched polyborosilazanes, ACS Appl. Mater. Interfaces 10 (2018) 28051-28061.

[47] Y. Yang, X. Ding, M. W. Urban, Chemical and physical aspects of self-healing materials, Prog. Polym. Sci. 49 (2015) 34-59.

[48] K. Imato, A. Takahara, H. Otsuka, Self-healing of a cross-linked polymer with dynamic covalent linkages at mild temperature and evaluation at macroscopic and molecular levels, Macromolecules 48 (2015) 5632-5639.

[49] A. Chao, J. Negulescu, D. Zhang, Dynamic covalent polymer networks based on degenerative imine bond exchange: tuning the malleability and self-healing properties by solvent, Macromolecules 49 (2016) 6277-6284.

[50] J. C. Halpin, Stiffness and expansion estimates for oriented short fiber composites, J. Compos. Mater. 3 (1969) 732-734.

[51] J. C. Affdl, J. L. Kardos, The Halpin-Tsai equations: A review, Polym. Eng. Sci. 16 (1976) 344-352.

[52] L. Wang, X. Jia, Y. Li, F. Yang, L. Zhang, L. Liu, X. Ren, H. Yang, Synthesis and microwave absorption property of flexible magnetic film based on graphene oxide/carbon nanotubes and Fe_3O_4 nanoparticles, J. Mater. Chem. A 2 (2014) 14940-14946.

[53] Y. Sun, J. Xu, W. Qiao, X. Xu, W. Zhang, K. Zhang, X. Zhang, X. Chen, W. Zhong, Y. Du, Constructing two-, zero-, and one-dimensional integrated nanostructures: an effective strategy for high microwave absorption performance, ACS Appl. Mater. Interfaces 8 (2016) 31878-31886.

[54] N. Zhou, Q. An, Z. Xiao, S. Zhai, Z. Shi, Rational design of superior microwave shielding composites employing synergy of encapsulating character of alginate hydrogels and task-specific components (Ni NPs, Fe_3O_4/CNTs), ACS Sustain. Chem. Eng. 5 (2017) 5394-5407.

[55] N. Li, G. Huang, Y. Li, H. Xiao, Q. Feng, N. Hu, S. Fu, Enhanced microwave absorption performance of coated carbon nanotubes by optimizing the Fe_3O_4 nanocoating structure, ACS Appl. Mater. Interfaces 9 (2017) 2973-2983.

[56] S. P. Pawar, M. Gandi, C. Saraf, S. Bose, Exceptional microwave absorption in soft polymeric nanocomposites facilitated by engineered nanostructures, J. Mater. Chem. C 4 (2016) 4954-4966.

Figures Captions

Fig. 1 (a) Illustration of self-healing effect driven by coupling thedynamic imine bonds at fractured surface, with the chemical structuredrawings for A_2 and B_3 monomers. Splicing of a collection of (b)PAM *'Tetris'* tiles*via* self-healing and (c) uniaxially compressing the spliced sheet to buckle. Optical microscopic images of PAM (d) before and (e) after self-healing. (f) Surface profiles for pure PAM before and after self-healing. Tensile testing results for PAM (g) at different healing time and (h) after healing for one, two, three cycles (H1, H2, H3).

Fig. 2 (a) Illustration of the structure for Fe_3O_4@MWCNTs/PAM nanocomposites with an inset SEM image for the Fe_3O_4@MWCNTs nanoparticles. Self-healing enabled (b) welding of cut dumbbell samplesand (c) tough bonding of films (1 mm in thickness) between the PAM and 15 wt% Fe_3O_4@MWCNTs/PAM. Tensile testing results for 15 wt% Fe_3O_4@MWCNTs/PAM nanocomposite (d) at different healing time and (e) after healing for one, two, three cycles (H1, H2, H3). (f) Schematic of EM wave absorption mechanism in nanocomposite. Reflection coefficient (RC) results for Fe_3O_4@MWCNTs/PAM nanocomposite in 8.2–12.4 GHz with nanofiller's concentrations of (g) 10 wt%, (h) 15 wt%, and (i) 20 wt%.

Fig. 3 The accelerated reformation processes for (a) PAM and (b) 15 wt% Fe_3O_4@MWCNTs/PAM nanocomposite at various compressive stresses, the scale bar is 5 mm. The tensile testing results after cyclic reformation at 5 MPa for (c) pure PAM for 3 h and (d) 15 wt% Fe_3O_4@MWCNTs/PAM nanocomposite for 15 h. (e) The sustainable roadmap of Fe_3O_4@MWCNTs/PAM nanocomposites. (f) ^1H NMR results for the solution after degradation. (g) Degradation efficiency tests for pure PAM and 15 wt% Fe_3O_4@MWCNTs/PAM nanocomposites. (h) Mechanical analysis results for the re-synthesised composite sampleand the original sample.

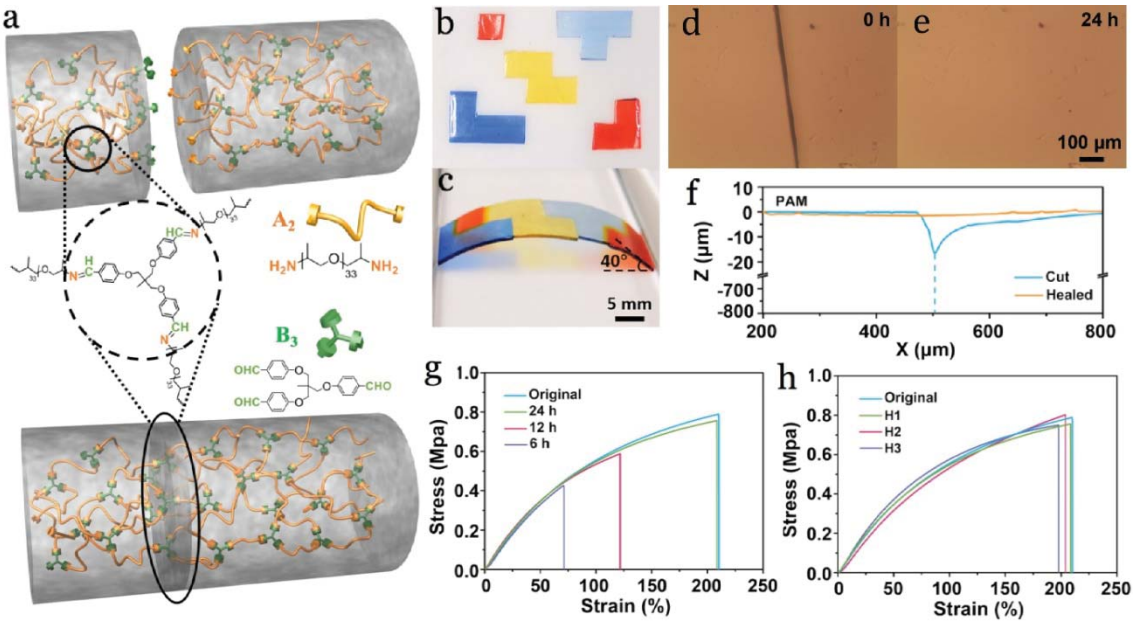

Fig. 1 (a) Illustration of self-healing effect driven by coupling thedynamic imine bonds at fractured surface, with the chemical structuredrawings for A_2 and B_3 monomers. Splicing of a collection of (b)PAM *'Tetris'* tiles*via* self-healing and (c) uniaxially compressing the spliced sheet to buckle. Optical microscopic images of PAM (d) before and (e) after self-healing. (f) Surface profiles for pure PAM before and after self-healing. Tensile testing results for PAM (g) at different healing time and (h) after healing for one, two, three cycles (H1, H2, H3).

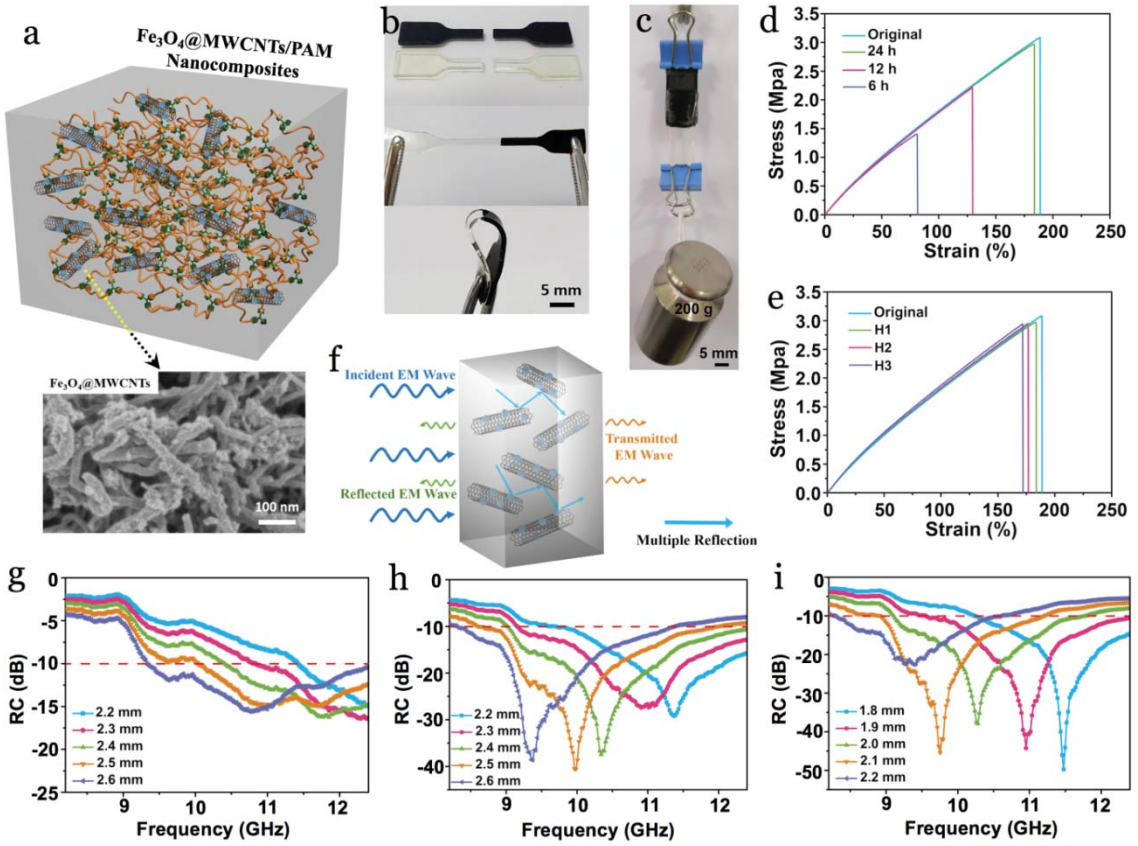

Fig. 2 (a) Illustration of the structure for Fe_3O_4@MWCNTs/PAM nanocomposites with an inset SEM image for the Fe_3O_4@MWCNTs nanoparticles. Self-healing enabled (b) welding of cut dumbbell samplesand (c) tough bonding of films (1 mm in thickness) between the PAM and 15 wt% Fe_3O_4@MWCNTs/PAM. Tensile testing results for 15 wt% Fe_3O_4@MWCNTs/PAM nanocomposite (d) at different healing time and (e) after healing for one, two, three cycles (H1, H2, H3). (f) Schematic of EM wave absorption mechanism in nanocomposite. Reflection coefficient (RC) results for Fe_3O_4@MWCNTs/PAM nanocomposite in 8.2–12.4 GHz with nanofiller's concentrations of (g) 10 wt%, (h) 15 wt%, and (i) 20 wt%.

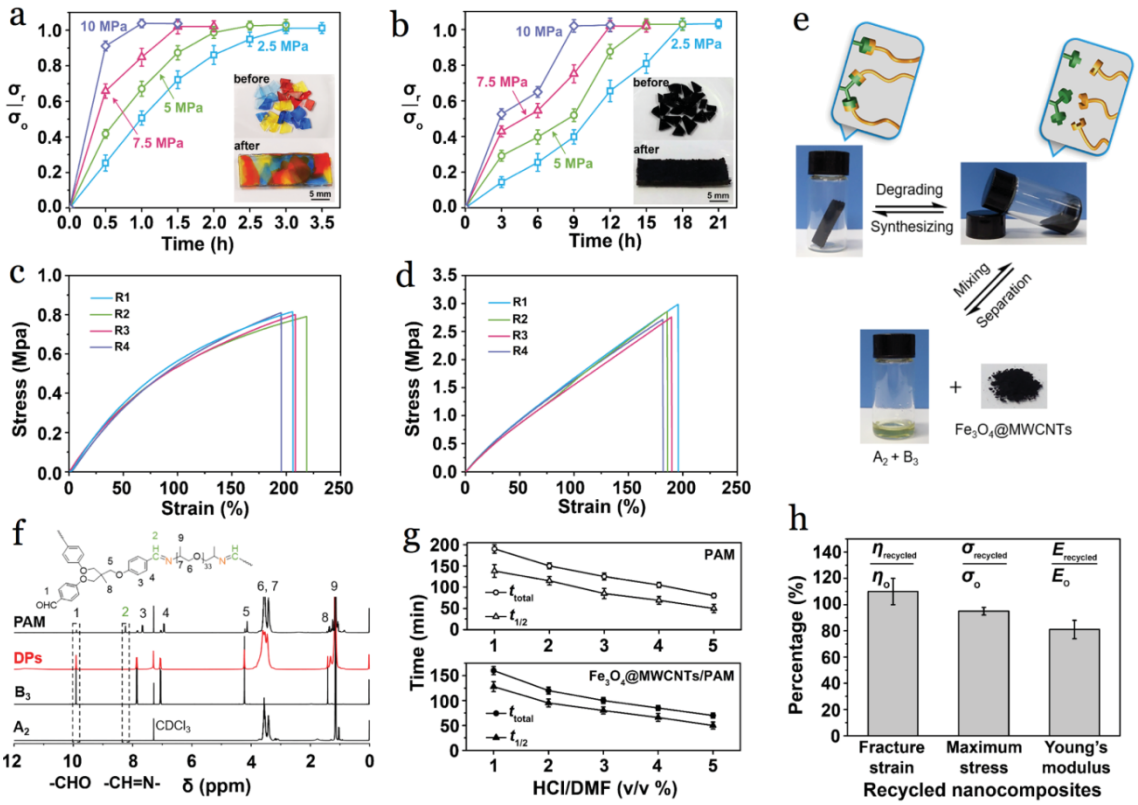

Fig. 3 The accelerated reformation processes for (a) PAM and (b) 15 wt% Fe_3O_4@MWCNTs/PAM nanocomposite at various compressive stresses, the scale bar is 5 mm. The tensile testing results after cyclic reformation at 5 MPa for (c) pure PAM for 3 h and (d) 15 wt% Fe_3O_4@MWCNTs/PAM nanocomposite for 15 h. (e) The sustainable roadmap of Fe_3O_4@MWCNTs/PAM nanocomposites. (f) ^{1}H NMR results for the solution after degradation. (g) Degradation efficiency tests for pure PAM and 15 wt% Fe_3O_4@MWCNTs/PAM nanocomposites. (h) Mechanical analysis results for the re-synthesised composite sampleand the original sample.

Supporting Information

Recoverable and Self-healing Electromagnetic Wave Absorbing Nanocomposites

Xingyi Dai[a], Yuzhang Du[a], Jiye Yang[a], Ding Wang[b], Junwei Gu[a], Yifan Li[b], Steven Wang[c], Ben B. Xu[b]*, and Jie Kong[a]*

[a]MOE Key Laboratory of Materials Physics and Chemistry in Extraordinary Conditions, Shaanxi Key Laboratory of Macromolecular Science and Technology, School of Science, Northwestern Polytechnical University, Xi'an, 710072, P. R. China

[b]Mechanical and Construction Engineering, Faculty of Engineering and Environment, Northumbria University, Newcastle upon Tyne, NE1 8ST, UK

[c]School of Chemical Engineering and Advanced Materials, Newcastle University, Newcastle Upon Tyne, Tyne and Wear NE1 7RU, UK

*Corresponding Authors, E-mail: kongjie@nwpu.edu.cn(J.K.), ben.xu@northumbria.ac.uk(B.X.)

Synthesis and Characterization

***Preparation of Fe_3O_4@MWCNTs nanofillers*:** Fe_3O_4 decorated multi-walled carbon nanotubes (Fe_3O_4@MWCNTs) were prepared following the reported procedures.[1] MWCNTs (2 g) were suspended in 100 mL concentrated nitric acid at 120 ^oC for 8 h under magnetic stirring. The mixture suspension was filtered, then the purified MWCNTs were washed with water to neutral pH, and dried at 80 ^oC in vacuum overnight. Next, we dispersed 0.5 g purified MWCNTs in 200 mL aqueous polyvinyl alcohol solutions (0.25%, w/v), where $FeCl_2$ $4H_2O$ (0.44 g, 2.17 mmol) and $FeCl_3$ $6H_2O$ (1.18 g, 4.33 mmol) were added together and ultra-sonicated for 30 min. Afterward, 5 mL NH_4OH aqueous solution (8 M) was added drop-wisely into the mixture to adjust pH to the range of 11–12. The mixture was kept at 60 ^oC to continue the reaction under nitrogen atmosphere for another 1 h with vigorously mechanical stirring. Finally, the Fe_3O_4@MWCNTs product was separated from the suspension and washed and dried at 80 ^oC.

***Characterizations*:** Fourier transform infrared spectroscopy (FT-IR) measurements were conducted on a Nicolet iS10 IR spectrometer (Thermo Scientific, USA) using the potassium bromide (KBr) method in the range of 4000–400 cm^{-1} at a resolution of 4 cm^{-1}.Powder X-ray diffraction (XRD) measurement was conducted on the X'Pert Pro powder diffractometer from PAN alytical (Rigaku, model D/max- 2500 system at 40 kV and 100 mA of Cu Kα). The X'Celerator Scientific RTMS detection unit was used for detection. X-ray photoelectron spectroscopy (XPS) measurement was conducted on a K-Alpha spectrometer (Axis Ultra, Kratos Analytical Ltd., U.K.) and the core level spectra were measured using amonochromatic Al Kα X-ray source (hν=1486.7 eV). The analyzer was operated at 23.5 eV pass energy and the analyzed area was 200–800μm in diameter. The lowest energy resolution is 0.48 eV (Ag 3d5/2). Binding energy was referenced to the adventitious hydrocarbon C1s line at 285.0 eV. The curve fitting of the XPS spectra was performed using the least-squares method.

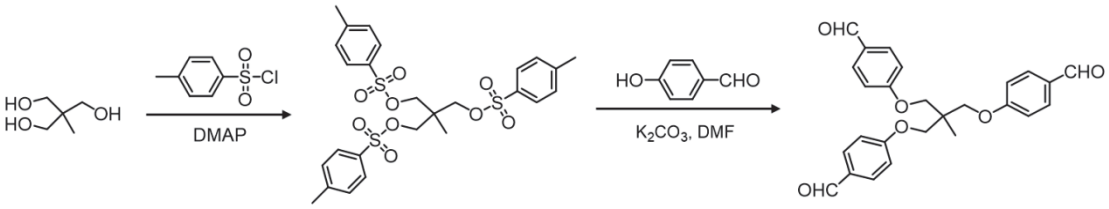

Fig. S1. The synthesis of 1, 1, 1-tris[(4-formylphenoxy)methyl]ethane.

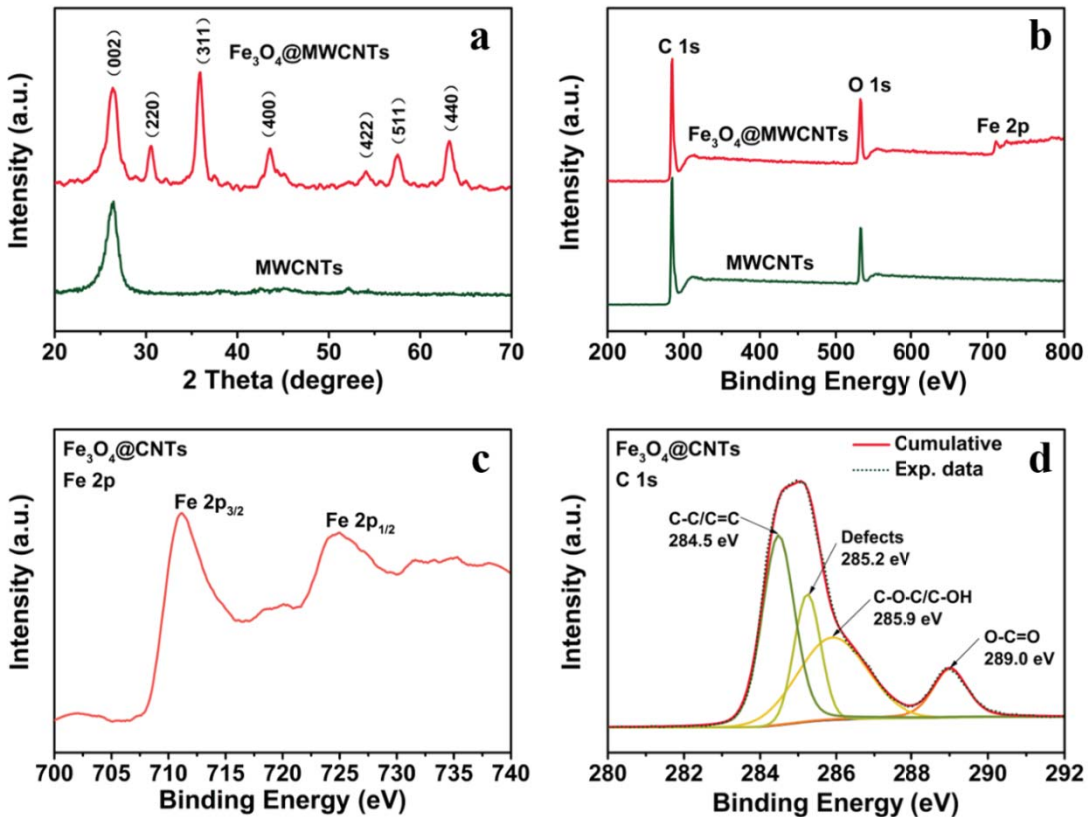

Fig. S2. (a) XRD patterns of MWCNTs, Fe_3O_4@MWCNTs; (b) XPS spectra of MWCNTs, Fe_3O_4@MWCNTs; (c) Fe 2p spectra of Fe_3O_4@MWCNTs; (d) C 1s spectra of Fe_3O_4@MWCNTs.

In Fig. S2a, the peak at 25° is assigned to (002) planes of the MWCNTs and Fe_3O_4@MWCNTs. Diffraction peaks at 30.00°, 35.45°, 43.10°, 53.44°, 57.04°, and 62.58° represent the Bragg reflection from (220), (311), (400), (422), (511), and (440) planes of the cubic spinel crystal structure of magnetite (JCPDS card No. 19-0629). The surface composition of the Fe_3O_4@MWCNTs nanocomposites was further investigated by XPS analysis, as shown in Fig. S2b. There are three peaks centered at around 285, 532 and 711 eV, which can be ascribed to the C 1s, O 1s and Fe 2p, respectively, in which signals of Fe and C element in Fe_3O_4@MWCNTswere observed.

Two broad peaks at binding energies of 711.1 and 725.0 eV are attributed to the Fe $2p_{3/2}$ and Fe $2p_{1/2}$ (Fig. S2c), demonstrating the oxidation states of Fe in the sample is Fe_3O_4.[2] In Figure S5d, the spectra of Fe_3O_4@MWCNTs are deconvoluted into four carbon components, in which the peaks located at 284.5, 285.2, 285.9 and 289.0 eV can be assigned to the C–C/C=C, defects of CNTs, C–O–C/C–OH and O–C=O, respectively.[3-5] All results further demonstrated that the Fe_3O_4 nanoparticles were successfully attached on the MWCNTs.

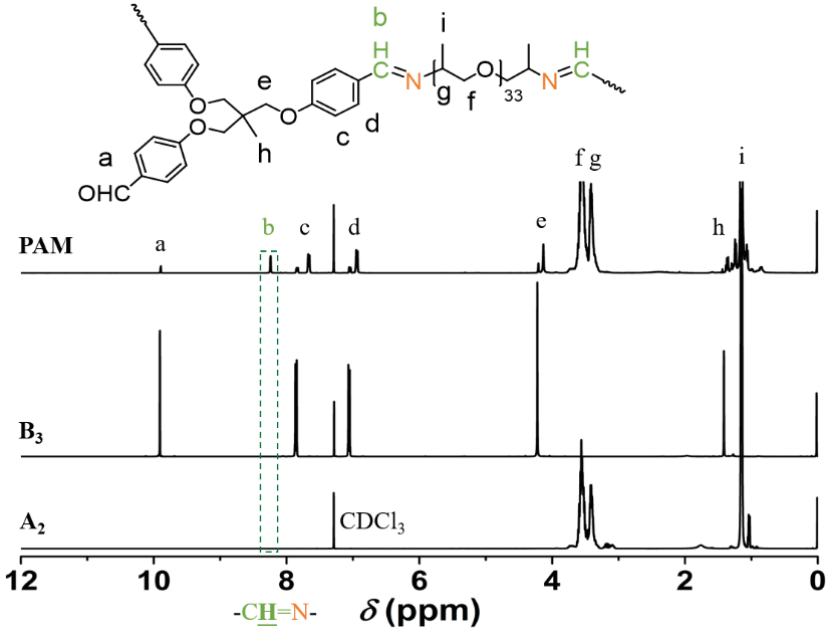

Fig. S3. ^{1}H NMR spectra of A_2, B_3, and PAM, the new presence of characteristic signal of the proton on -CH=N- bond at 8.24 ppm indicating the success synthesis of PAM.

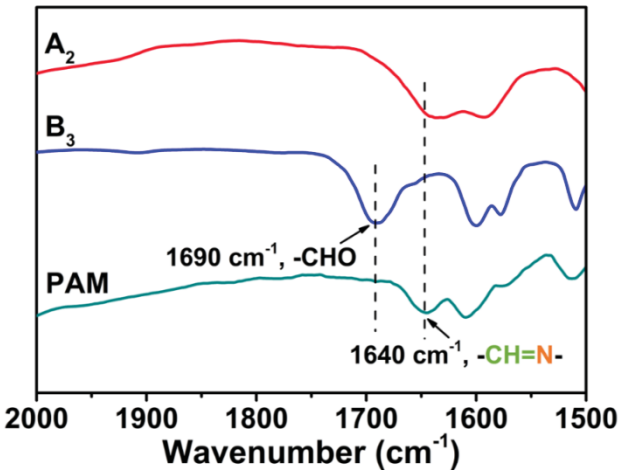

Fig. S4.FT-IR spectra range from 2000 cm^{-1} to 1500 cm^{-1} of A_2, B_3, as well as PAM demonstrating the success formation of imine bonds.

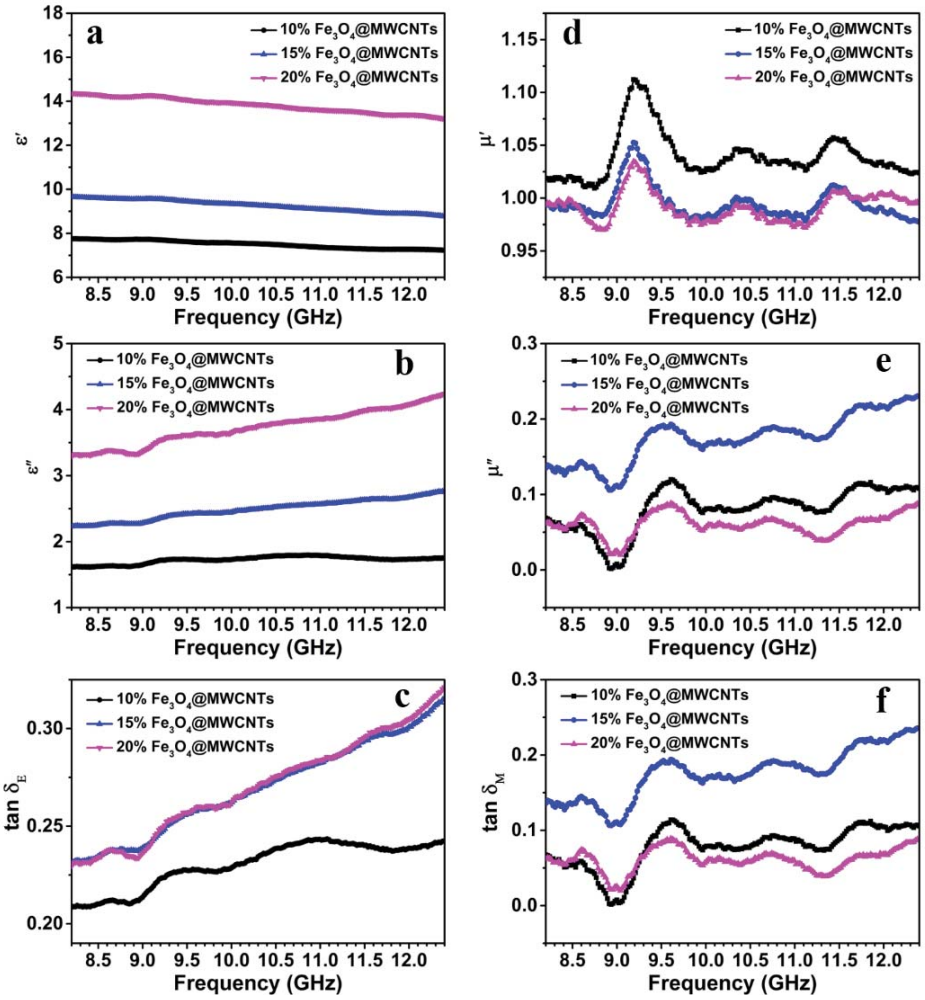

Fig. S5. Electromagnetic parameters of Fe_3O_4@MWCNTs/PAM nanocomposites with various Fe_3O_4@CNTs mass fraction (10 wt%, 15 wt%, and 20 wt%) in the frequency range of 8.2–12.4 GHz, (a) real parts (□□) of complex permittivity, (b) imaginary parts (□□) of complex permittivity, (c) dielectric loss tangent (tan δ_E), (d) real parts (μ□) of complex permeability, (e) imaginary parts (μ□) of complex permeability as well as (f) magnetic loss tangent (tan δ_M).

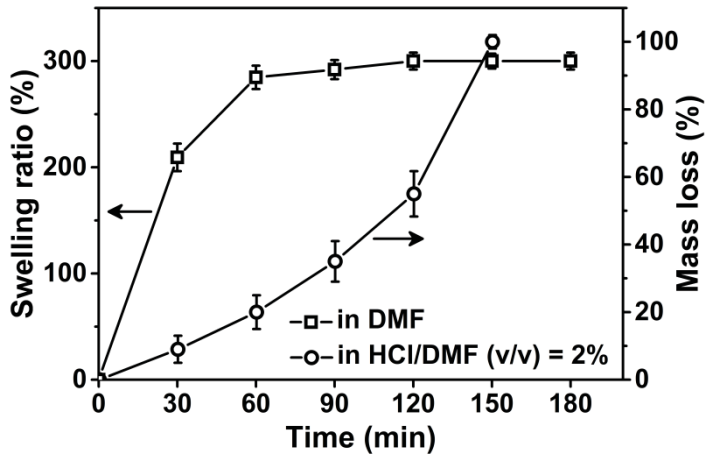

Fig. S6. Comparison of the behaviors of pure PAM (100 mg) in DMF with and without presence of HCl.

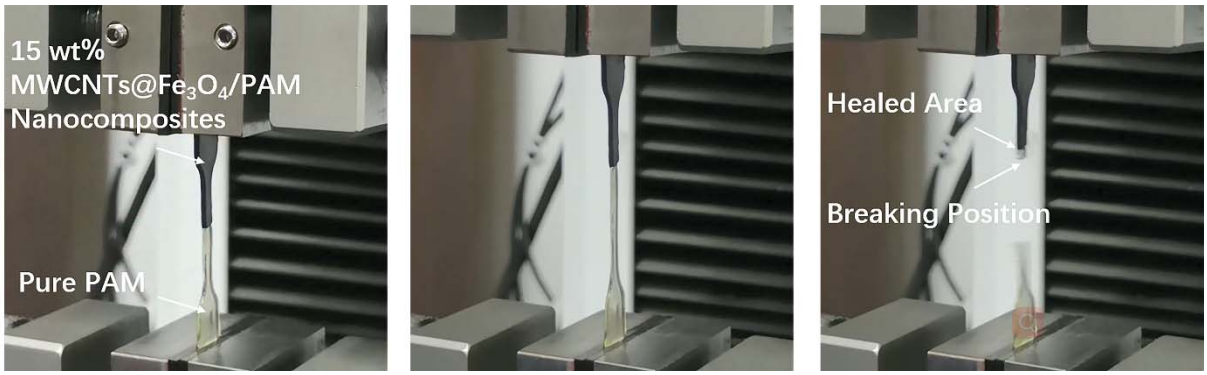

Fig. S7. Tensile testing process of the healed sample between pure PAM and 15 wt% Fe_3O_4@MWCNTs/PAM

References:

[1] Y. He, L. Huang, J. Cai, X. Zheng, S. Sun, Structure and electrochemical performance of nanostructured Fe_3O_4/carbon nanotube composites as anodes for lithium ion batteries, Electrochim. Acta 55 (2010) 1140-1144.

[2] Y. Liu, W. Jiang, Y. Wang, X. J. Zhang, D. Song, F. S. Li, Synthesis of Fe_3O_4/CNTs magnetic nanocomposites at the liquid-liquid interface using oleate as surfactant and reactant. J. Magn. Magn. Mater. 321 (2009) 408-412.

[3] K. Yang, M. Gu, Y. Guo, X. Pan, G. Mu, Effects of carbon nanotube functionalization on the mechanical and thermal properties of epoxy composites, Carbon47 (2009) 1723-1737.

[4] P. Liu, Y. Huang, J. Yan, Y. Yang, Y. Zhao, Construction of CuS Nanoflakes vertically aligned on magnetically decorated graphene and their enhanced microwave absorption properties. ACS Appl. Mater. Interfaces 8 (2016) 5536-5546.

[5] T. Wu, Y. Liu, X. Zeng, T. Cui, Y. Zhao, Y. Li, G. Tong, Facile hydrothermal synthesis of Fe_3O_4/C core-shell nanorings for efficient low-frequency microwave absorption. ACS Appl. Mater. Interfaces 8 (2016) 7370-7380.